NiAlxFe2–xO4 mixed oxide catalysts for methane reforming with CO2: Effect of Al vs Fe contents and precursor salts

Rafik Benrabaa, Martine Trentesaux, Pascal Roussel, Annick Rubbens, Rose-Noelle Vannier, Axel Löfberg

Journal of CO2 Utilization 67 (2023) 102319

Contents lists available at ScienceDirect

Journal of CO2 Utilization

journal homepage: www.elsevier.com/locate/jcou

$NiAl_xFe_{2-x}O_4$ mixed oxide catalysts for methane reforming with CO_2: Effect of Al vs Fe contents and precursor salts

Rafik Benrabaa [a,b,*], Martine Trentesaux [c], Pascal Roussel [c], Annick Rubbens [c], Rose-Noëlle Vannier [c], Axel Löfberg [c]

[a] Laboratoire de Physico-Chimie des Matériaux, Faculté des Sciences et de la Technologie, Université Chadli Bendjedid-El Tarf, B.P 73, El Tarf 36000, Algeria
[b] Laboratoire de Matériaux Catalytiques et Catalyse en Chimie Organique, Faculté de Chimie, USTHB, BP32, El-Alia, 16111 Bab Ezzouar, Alger, Algeria
[c] Univ. Lille, CNRS, Centrale Lille, Univ. Artois, UMR 8181 - UCCS - Unité de Catalyse et Chimie du Solide, F-59000 Lille, France

ARTICLE INFO

Keywords:
Spinel structure
Mixed oxides
Characterization
Dry reforming of methane

ABSTRACT

$NiAl_xFe_{2-x}O_4$ ($0 \leq x \leq 2$) was synthesized, characterized and evaluated in methane reforming with CO_2 without any pretreatment. It was shown that the nature of the precursor has a significant effect on the structural, textural and reactivity properties. The cell parameters decrease with increasing Al-content which can be explained by the partial substitution of Fe^{3+} ions (~0.63 Å in tetrahedral site and ~0.78 Å and high spin in octahedral site) by Al^{3+} ions (~0.53 Å) either in the tetrahedral or the octahedral sites. If, on the one hand, the catalytic activity of the aluminum compound exhibits high CH_4 and CO_2 conversions as well as excellent syngas selectivity, on the other hand, a poor activity is observed for $NiFe_2O_4$ whatever the precursors. For low temperatures ($T < 750$ °C), powders prepared with chlorides are more active than powders prepared with nitrates. However, this behavior mitigates at high temperature. $NiAl_2O_4$ issued from nitrate precursors shows the best catalytic performances. Negligible contributions to WGS Reaction are illustrated by H_2/CO ratios close to stoichiometry. The intermediate $FeAl_2O_4$ spinel phase plays an important role as catalytic precursor in the in-situ production of Ni° nanoparticles, highly dispersed and less prone to coke formation in spite of the severe reaction conditions. A lack of affinity of Al-species to combine with Ni° to form detrimental Ni-Al alloy is proposed to explain the good performances. Strong interactions developed between metallic active sites and mixed oxides substrates allow the stabilization and improvement of catalytic performances in dry reforming of methane.

1. Introduction

Syngas (H_2 and CO) is an extremely important commodity in the petroleum and chemical industry since it is an intermediate for synthesizing various chemicals, such as methanol, ammonia, diesel fuels or synthetic gasoline [1] or can directly be used as H_2 source. Several ways are used for syngas production such as the steam reforming of natural gas or gasification of coal. However, these processes are characterized by a high consumption of fossil fuels and high energy needs, which are provided by combustion of additional fossil fuels. The partial oxidation of methane (POM) or the dry reforming of methane (DRM) are attractive alternative routes [2]. Among these, DRM with carbon dioxide is the most attractive industrial route for the production of syngas ($CO_2 + CH_4 \leftrightarrow 2CO + 2\ H_2$, $\Delta H°_{298} = 247$ kJ/mol). It has received considerable interest for several reasons: (i) an increased interest in the effective utilization of the greenhouse gas carbon dioxide, (ii) an interesting way to use biogas, containing CH_4 and CO_2, resulting from anaerobic digestion of biomass and (iii) a hydrogen to carbon monoxide H_2/CO ratio close to the ideal value of 1 [3,4].

DRM is carried out in the presence of supported transition metal catalysts. Among these, noble metals (Rh, Pd. etc) have excellent activities and resistance to coke formation but are not conceivable given their very high costs. Nickel is the only viable alternative from an economic point of view [5–8]. However, fears about the toxicity of this metal need the search of alternative materials with catalytic performances allowing the reduction of the amount of nickel used. The major problem associated with CO_2 reforming on nickel-based catalysts is the rapid carbon deposition on the catalyst by the dissociation reaction of carbon monoxide ($2CO \leftrightarrow CO_2 + C$) and / or the decomposition reaction of methane ($CH_4 \leftrightarrow C + 2\ H_2$) [9–11]. The formation of an inactive

* Corresponding author at: Laboratoire de Physico-Chimie des Matériaux, Faculté des Sciences et de la Technologie, Université Chadli Bendjedid-El Tarf, B.P 73, El Tarf 36000, Algeria.
E-mail address: r.benrabaa@univ-eltarf.dz (R. Benrabaa).

https://doi.org/10.1016/j.jcou.2022.102319
Received 28 March 2022; Received in revised form 31 October 2022; Accepted 3 November 2022

carbon-based surface, which blocks active sites and inhibits the reaction, is favored on large size nickel metal particles (agglomerates). Thus, to limit sintering and coke formation, the stabilization of nanoscale particles is necessary. For this purpose, it is important to master their preparation perfectly and to know precisely their structural and textural characteristics.

One of the suggested solutions is to deposit nickel on a support (SiO_2, Al_2O_3 or MgO) [12,13]. The role of the support is to allow a better dispersion of the active phase and promote the formation of fine metallic particles. Another possibility to increase the dispersion of metallic particles on the surface of a catalyst is to incorporate the active nickel in a well-defined structure such as spinel, perovskite, pyrochlore, hydrotalcite, etc., i.e. structural types well-known to form solid solutions with nickel.

In this frame, compounds with the spinel structure are excellent candidates. They are already used in many applications: in electronics for their ferromagnetic properties, in catalysis for the reduction of NOx, the decomposition of alcohols and the reforming of hydrocarbons [14–18].

Spinels are mixed oxides of general formula AB_2O_4 where A denotes a bivalent cation and B denotes a trivalent cation. The oxygen ions, which are larger compared to the cations A and B, form a cubic lattice with centered faces (cfc) in which the metal cations A and B occupy the tetrahedral and the octahedral sites, respectively. There are two kinds of ideal spinels, namely the direct (or normal) and inverse spinels. In the direct one, the cations A^{2+} occupy 1/8 of the tetrahedral sites [Td] while the trivalent cations B^{3+} occupy half of the octahedral sites [Oh]. The general formula of this compound can therefore be written: $\left[A^{2+}_{Td}\right]\left[B^{3+}_{Oh}\right]_2 \quad \left[O^{2-}\right]_4$. In the second type, the network can be partially or totally inverted. The general formula of such a network can be written: $(A_{1-\gamma}B_{\gamma})\ [A_{\gamma}B_{2-\gamma}]O_4$ where γ is called the inversion degree, and represents the fraction of divalent cations in octahedral position [O_h]. For $\gamma = 0$ the spinel is normal, for $0 < \gamma < 1$ the network is partially inverted and for $\gamma = 1$ the network is completely inverted and corresponds to the formula: $\left[B^{3+}_{Td}\right] \quad \left[A^{2+}_{Oh}B^{3+}_{Oh}\right] \quad \left[O^{2-}\right]_4$. In the latter case, all the divalent cations are in the octahedral position and half of the trivalent cations are in the tetrahedral position and the other half is in the octahedral position. The major advantage of the spinel-type oxides is their tolerance to the partial substitution of the A- and B-sites by cations of different nature, leading to a wide variety of compounds characterized by electronic (unusual oxidation state of the B-site cation) and structural defects (vacancies and/or mobility of lattice oxygen), owing to their non-stoichiometry which plays an important role in catalytic processes. Thus, their catalytic activity depends essentially on two parameters: the degree of substitution of each cation and the degree of inversion of the spinel structure.

Iron-nickel spinel $NiFe_2O_4$ adopts an inverse spinel structure. In this structure, the trivalent cations Fe^{3+} occupy both the octahedral sites Fe [Oh] and the tetrahedral sites Fe[Td], while the divalent cations Ni^{2+} are all in an octahedral environment Ni[Oh] [19]. Aluminum-nickel spinel is a partially inverse spinel oxide which can be written $[Ni_{0.16}Al_{0.84}][Ni_{0.84}Al_{1.16}]O_4$ where inversion degree $\gamma = 0.84$ [19]. The solid solution between both spinels $NiFe_2O_4$ and $NiAl_2O_4$ has potential applications due to their unique magnetic and electrical properties which undergo drastic changes depending on cations distribution [19]. In this solid solution, according to Kamali et al., as Al is incorporated the $NiFe_2O_4$ system, it would firstly preferentially substitutes Fe species in octahedral sites and then, when all Fe at octahedral sites would have been replaced, aluminum would substitute Fe at tetrahedral positions [20].

In our previous works, efforts had been concentrated over the "simple" binary different spinels: $NiFe_2O_4$ and $NiAl_2O_4$. Both compounds showed a completely different behavior toward CH_4/CO_2 reaction. It was shown that the unreduced aluminate spinel $NiAl_2O_4$ prepared by coprecipitation route, had a significant catalytic activity in the DRM reaction although carbon deposition was observed [11]. In contrast, $NiFe_2O_4$ showed a fairly low activity but with almost zero coke deposition [9,21]. In order to combine the advantages of both spinels, $NiFe_2O_4$ and $NiAl_2O_4$, and to find alternative catalysts, which can be more resistant against coke formation in dry reforming of methane, a series of ternary spinel-type oxides $NiAl_xFe_{2-x}O_4$ $(0 \leq x \leq 2)$ were studied in this work. The present paper reports the effect of (i) Al-content and (ii) nature of salts used as reagent (nitrates or chlorides) on the textural and structural properties of the ternary spinel-type oxides. The behavior in reducing atmosphere and the catalytic properties in dry reforming of methane were also investigated.

2. Experimental

2.1. Preparation of catalysts

A series of $NiAl_xFe_{2-x}O_4$ $(0 \leq x \leq 2)$ ternary spinel oxides were synthesized by coprecipitation method using nitrates and chlorides as reagents. The synthesis was carried out at ambient temperature by addition of sodium hydroxide 2 M, up to pH= 10, to an aqueous solution of hydrates of nickel, aluminum and iron chlorides or nitrates. After washing by distilled water and drying at 80 °C, the precursors were calcined in air flow during 4 h at 800 °C. The powders elaborated from chloride salts are noted x(Cl^-) and those issued from nitrates are named x (NO_3^-) (with x corresponding to the Al-content). The equations of reactions are given below:

$$NiCl_2.6\ H_2O + x\ AlCl_3.6\ H_2O + (2\text{-}x)\ FeCl_3.6\ H_2O + 8NaOH \rightarrow NiAl_x\text{-}Fe_{2-x}O_4 + 8NaCl + 22\ H_2O \quad (1)$$

$$Ni(NO_3^-)_2.6\ H_2O + x\ Al(NO_3^-)_3.9\ H_2O + (2\text{-}x)\ Fe(NO_3^-)_3.9\ H_2O + 8NaOH \rightarrow NiAl_xFe_{2-x}O_4 + 8(NaNO_3) + 28\ H_2O \quad (2)$$

2.2. Physicochemical analyses

Several physicochemical methods were used for the characterization of $NiAl_xFe_{2-x}O_4$ $(0 \leq x \leq 2)$ catalysts before and after heating treatment.

X-ray powder diffraction (XRD) was performed on a Bruker AXS D8 Advance diffractometer working in Bragg-Brentano geometry using Cu K_α radiation ($\lambda = 1.5418$ Å), equipped with a 1D LynxEye Silicon Strip detector recording 3° in one shot. Patterns were collected at room temperature, in the $2\theta = 10$–90° range, with a 0.02° step and a 1 s counting time per step. The EVA 5.1, 2019, Bruker AXS GmbH, Karlsruhe, Germany software was used for phase identification. The unit cell parameters and crystallite size were evaluated with the Jana2006 program [22]. To study the reducibility of the catalyst, in situ XRD was carried out under hydrogen atmosphere (3% H_2 in N_2) (H_2-HT-XRD) at variable temperatures up to 800 °C on the same type of diffractometer equipped with an Anton-Par XRK 900 chamber and a LynxEye detector. Diagrams were collected every 25 °C at 0.1 °C/s heating rate, the counting time being chosen to collect a diagram in 15 min in the 10–90° 2θ range. The sample was deposited on a platinum sheet and H_2 was flowed in the chamber (5 L/h). After measurement, all samples were cooled down to room temperature at 0.3 °C/s cooling rate.

TG-DTA carried out under air flow before calcination was performed on a SETARAM TG-92. 20 mg sample was heated at 5 °C/min from 25° to 1000°C. *In-situ* TGA under H_2 atmosphere was performed on samples previously calcined under air flow at 800 °C using a Hiden Isochema gravimetric analyzer (model IGA-003) under 5% H_2 in Ar flow from 25° to 500°C. Ca. 20 mg of sample was used. Measurements at 400 °C for 5 h under H_2 atmosphere were also carried out.

Laser Raman Spectroscopy (LRS) was performed with Spectra Physics krypton ion laser at room temperature using the 647.1 nm excitation line. The beam was focused onto the samples using the macroscopic configuration of the apparatus. To avoid damage due to

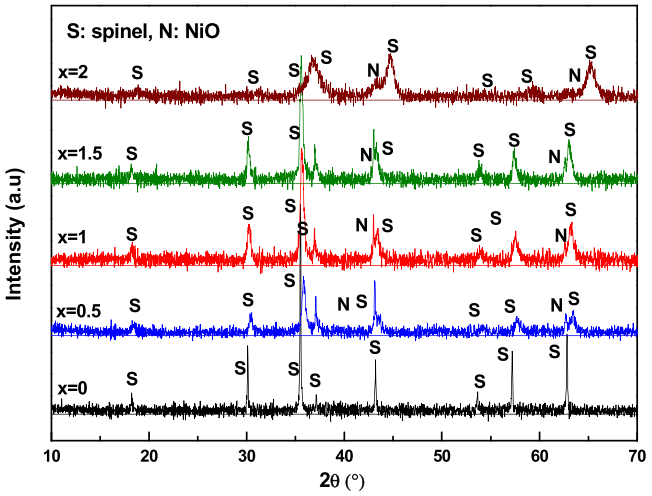

Fig. 1. XRD patterns of $NiAl_xFe_{2-x}O_4$ ($0 \leq x \leq 2$) spinel catalysts prepared from chlorides salts.

laser heating, all compounds were studied at a very low laser power (3 mW on the sample). Four accumulations were used in each spectral range. No damage of the material by the laser was observed. The scattered light was analyzed with an XY Raman Dilor spectrometer equipped with an optical multichannel charge coupled device liquid nitrogen-cooled detector. The spectral resolution was 0.5 cm^{-1} in the 200–1500 cm^{-1} range. Acquisition and data processing were performed with the LABSPEC software.

Attenuated Total Reflection Infra-Red Spectra (IR-ATR) were recorded at room temperature using a Perkin Elmer model 400 in transmission mode, in the range from 350 to 4000 cm^{-1}.

The specific surface area (S_{BET}) of the catalysts was determined by nitrogen adsorption at − 196 °C with a Micromeritics ASAP2010 apparatus.

Scanning electron microscopy (SEM) coupled to X-ray energy dispersive microanalysis (EDX) were carried out on HITACHI 4100 S apparatus at 6 kV. Catalysts were ground as fine particles and mechanically dispersed on an electrically conductive carbon tape which was placed on an aluminum disc.

X-ray photoelectron spectroscopy (XPS) was carried out on Escalab 220 XL spectrometer (Vacuum Generators). A monochromatic Al Kα X-ray source was used and electron energies were measured in the constant analyzer energy mode. The pass energy was 100 eV for the survey of spectra and 40 eV for the single element spectra. All XPS binding energies were referred to C*1 s* core level at 285 eV. The angle between the incident X-rays and the analyzer was 58°, photoelectrons being collected perpendicularly to the sample surface. Spectra were analyzed with the CasaXPS software.

The reducibility of samples was studied by temperature programmed reduction by hydrogen (H_2-TPR), which was carried out on Micromeritics-Autochem II 2920 with a TCD detector to monitor the H_2 consumption. After calibration of H_2 on the TCD, the sample displayed in a U-shaped quartz reactor was pre-treated in argon, and heated at 5 °C/min from 25° to 1000°C in 5% H_2 in Ar gas mixture.

2.3. Catalytic tests

The CO_2 reforming of methane was carried out in a fixed-bed quartz flow reactor at atmospheric pressure in the temperature range 650–800 °C. The sample (ca. 200 mg) was thoroughly mixed with SiC powder, before loading in the reactor. The total quantity of catalyst and SiC was kept constant (1000 mg) for all experiments. A mixture of CH_4 and CO_2 (CH_4:CO_2:He:Ar = 20:20:10:50) with total flow 100 mL/min was introduced into the reactor and the reaction was started by increasing the temperature from room temperature up to 800 °C at 5 °C/min heating rate. All effluents were analyzed by online mass spectrometry (Prisma200, Pfeiffer Vacuum). After experiments, the catalyst was re-oxidized under 2% O_2 in He (50 mL/min) at 700 °C for 30 min, to determine the amount of carbon deposited on the surface. This allowed to check that the mass balance calculated by gas phase analysis of product during reaction fitted within a reasonable experimental error.

Table 1
Chemical composition evaluated by EDX and XPS analysis and specific surface area of catalysts calcined at 800 °C.

	S_{BET} (m^2/g)	EDX		XPS				
		Al: Ni	Fe: Ni	Al: Ni	Fe: Ni	O/ Ni	O/ Al	O/ Fe
$NiFe_2O_4$ (Cl^-)	10	–	2.3	–	5.7	2.5	–	0.4
$NiAl_{0.5}Fe_{1.5}O_4$ (Cl^-)	26	0.4	1	0.1	0.8	1	16.2	1.4
$NiAlFeO_4$(Cl^-)	38	0.5	1	0.3	0.7	1.2	3.8	1.6
$NiAl_{1.5}Fe_{0.5}O_4$ (Cl^-)	45	0.5	0.6	0.3	0.6	1.1	3.5	1.7
$NiAl_2O_4$ (Cl^-)	101	1.9	–	0.5	–	2	3.9	–
$NiFe_2O_4$ (NO_3^-)	2	–	2	–	–	–	–	–
$NiAlFeO_4$ (NO_3^-)	25	0.6	1	0.1	0.8	0.9	19.3	1.3
$NiAl_2O_4$ (NO_3^-)	149	1.4	–	–	–	–	–	–

3. Results and discussion

3.1. Thermal analysis by TG-DTA

TG-DTA thermograms recorded under air on sample before calcination are given in Fig. 1(S) in Supporting Information. For all the samples, the species responsible for the mass loss are water, carbonates and nitrates. Mainly three or four steps were noticed for formulations from chlorides salts with a significant weight loss probably linked to the departure of the adsorbed water and the decomposition of carbonate followed by a smaller weight loss around 500–600 °C which could be associated to departure of carbonate. A plateau seems to be reached at 800 °C in chloride cases.

In the case of nitrates, there are mainly three stages of weight loss, the last loss being located around 300 °C, a stability being reached at 550 °C.

However, regardless of the salt used, the highest total weight loss was recorded for precursor prepared from chlorides (38% for x = 2(Cl^-) against 33.5% for x = 2 (NO_3^-)).

Although, the recorded thermograms showed that the use of nitrates salts provided a thermic stability at lower temperatures: at ~550 °C for x = 2 (NO_3^-) against ~ 800 °C for $NiAl_xFe_{2-x}O_4$ (Cl^-), to be in the same conditions, it was decided to calcine $NiAl_xFe_{2-x}O_4$ ($0 \leq x \leq 2$) solids issued from chlorides and nitrates precursors at 800 °C.

3.2. Bulk and surface properties by EDS, XPS and B.E.T

The Bulk and the surface chemical properties of the $NiAl_xFe_{2-x}O_4$ ($0 \leq x \leq 2$) issued from chloride and nitrate precursors after calcination at 800 °C for 4 h under air flow were examined by EDX, XPS and B.E.T measurements. The obtained data are summarized in Table 1. The estimated Al/Ni and Fe/Ni atomic ratios, using EDX analysis, are almost similar to the theoretical values for the binary formulations (x = 0 and x = 2) prepared from both precursors suggesting a fairly homogenous distribution of the Ni, Al or Fe metals during precipitation. In contrast, an excess of nickel is observed for the ternary systems. At the surface, as shown by XPS, the enrichment in nickel is even more pronounced, even for $NiAl_2O_4$ composition (x = 2). However, an enrichment in iron is shown for the $NiFe_2O_4$ (x = 0) composition prepared from chloride precursors. Ni and Fe segregations strongly suggest the formation at the spinel surface of free NiO for sample containing aluminum and free

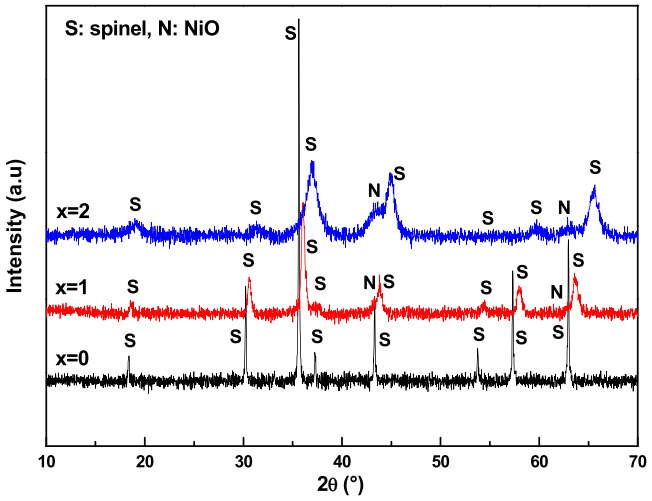

Fig. 2. XRD patterns of $NiAl_xFe_{2-x}O_4$ (x = 0; 1; and 2) spinel catalysts prepared from nitrates salts.

Fe_2O_3 in case of $NiFe_2O_4$ (x = 0). This was confirmed by XPS spectroscopy. For the Ni*2p*$_{3/2}$ peaks (Fig. 2(S)-7S, see SI), similar shapes are observed whatever the x value. They are composed of a main peak located at 855.4 eV and a relatively intense satellite peak at about 6.5 eV. The existence of such a satellite is characteristic of the oxidation state (+II) of nickel [23,24]. According to literature data [23,24], the decomposition of these spectra shows the presence of Ni (II+) in NiO by the lines located at ≈ 853.9; 855.1; 860.9 and 867.1 eV. $Ni(OH)_2$ hydroxide (Ni, II+) shows values close to that of NiO oxide, but its presence can be excluded because the calcination is carried out at 800 °C where the total transformation of $Ni(OH)_2$ hydroxide into oxide is ensured. The peaks situated at ≈ 856; 862 and 866.9 eV can be attributed to nickel in the spinel structure. It is important to note that the introduction of Al-species does not cause any variation in Ni*2p3/2* binding energies (855.4 eV) of $NiAl_xFe_{2-x}O_4$ mixed oxides thus explaining the stable position of Ni-species.

The Fe*2p3/2* spectra (Fig. 8S-12S, see SI) displays the same peak shapes for x = 0.5 (Cl^-), x = 1 (Cl^-), x = 1 (NO_3^-) and x = 1.5 (Cl^-). XPS peaks of Fe*2p3/2* (at 710.8 ± 0.3 eV) showed that the oxidation states of Fe species were (III+) in the mixed spinel oxides. In contrast, an additional component was observed at 719.5 eV (Fig. 8S) for the aluminum free sample (x = 0 (Cl^-)) which is characteristic of the presence Fe (III) from Fe_2O_3 (α or γ) [23,24]. It was not possible to specify the kind of Fe_2O_3 oxide (α or γ) since the corresponding binding energy for both oxides is practically the same. It is worth noting that, after decomposition XPS spectra of Fe*2p3/2* species for all mixed formulations (Fig. ^{9}S–^{12}S, see SI), we could observe an additional line located at ~709 eV attributed to Fe species in the oxidation state II+ (Fe^{2+}). This would suggest the presence of Fe^{2+} in the structure which could be related to the partial substitution of Ni^{2+} in the octahedral sites and explain the formation of NiO as a second phase. In contrast, all Al*2p* photopeaks could be deconvoluted with a single component (Figures ^{13}S–^{17}S, see SI) located at 73.8 eV for low Al-content (x = 0.5 and 1) issued from (Cl^-) or (NO_3^-) precursors and at ~74.4 eV for high Al-content (x = 1.5 and 2). These values (73.8–74.4 eV) are typical for Al (III). It is worth noting that the Al*2p* binding energy in α-Al_2O_3 is 74.2 eV. However, given XPS quantifications which revealed a surface poor in Al-species for all compositions, (Table 1), the hypothesis of Al_2O_3 at the subsurface was ruled out.

For the lattice oxygen, it can be observed that $NiFe_2O_4$ (Cl^-) presented a surface poor in O species evaluated by the low O/Ni and O/Fe ratios compared to the expected stoichiometry (Table 1). In contrast, an excess of lattice oxygen confirmed by the high O/Al ratio on the surface of the other systems was observed. The mixed intermediary formulations

Table 2
XRD phases and crystallographic parameters of catalysts calcined at 800 °C.

Catalysts	Phases	%	a (Å)[a]	C_S (nm)[a]
$NiAl_{0.5}Fe_{1.5}O_4$ (Cl^-)	S*	86.1	8.301(2)	28.9
	NiO	13.9	4.178(3)	54.5
$NiAlFeO_4$ (Cl^-)	S*	91.6	8.286(2)	24.3
	NiO	8.4	4.181(3)	92.6
$NiAl_{1.5}Fe_{0.5}O_4$ (Cl^-)	S*	78.7	8.274(2)	22.3
	NiO	21.3	4.179(3)	91.4
$NiAl_2O_4$ (Cl^-)	S*	90	8.056(5)	7
	NiO	10	4.176(5)	31
$NiAlFeO_4$ (NO_3^-)	S*	89.8	8.263(2)	24.9
	NiO	10.2	4.180(2)	14.8

* Spinel-type phase

(0.5 ≤x ≤ 1.5) show a surface richer in O species but the amounts remain low compared to binary system $NiAl_2O_4$ (Cl^-) (Table 1). The oxygen enrichment for these formulations coincides suitably with the values of the binding energies which confirmed the presence of a phase mixture containing NiO and the spinel phase, since O species exist in both NiO and spinel structures.

The specific surface areas are also given in Table 1. S_{BET} obtained for binary ferrite spinel with (Cl^-) or (NO_3^-) precursors at 800 °C were very low (<10 m^2/g). Hence, it's clear that Al-incorporation improves the specific surface areas of mixed oxides structures. It is also worth noting a significant impact of the nature of precursors used for the synthesis for the aluminate spinel $NiAl_2O_4$ with a $S_{B.E.T}$ = 149 m^2/g for $NiAl_2O_4$ (NO_3^-) against 101 m^2/g for $NiAl_2O_4$ (Cl^-).

3.3. Structural properties of catalysts by XRD, Raman and IR

X-Ray Diffraction, LRS Raman spectroscopy and Infra-red analyses were used to ascertain structural properties of catalysts. Figs. 1 and 2 show the X ray powder diffraction patterns of $NiAl_xFe_{2-x}O_4$ (0 ≤x ≤ 2) prepared from chloride and nitrate salts and calcined at 800 °C, respectively. In all cases, the patterns present peaks corresponding to the cubic spinel structures with space group $Fd\bar{3}m$. However, whereas a single phase corresponding to the spinel ferrite (*PDF 00–010–0325*) was observed for the $NiFe_2O_4$ formulation (x = 0), for the other catalysts (0.5 ≤x ≤ 2), two additional peaks were observed. They were attributed to the cubic crystalline structure of NiO (*PDF 01–089–5881*) in good agreement with XPS analysis. For all formulations, no indication of oxides such as Fe_2O_3 or Al_2O_3 could be observed.

Beside full pattern matching used for the calculation of the lattice parameters (a) and the crystallites sizes (C_S), Rietveld refinement of patterns was carried out to propose phase quantification. The structural models corresponding to NiO (reference ICSD nr 28834) and $NiFe_{1.5}Al_{0.5}O_4$ (ref ICSD nr 185298) were introduced in the refinement with aluminum equally distributed in both tetrahedral and octahedral sites and nickel in the octahedral site only. Site occupancies were not refined at that stage. The obtained values are given in Table 2 and their variations with Al-content, for the catalysts prepared from chloride salts, are shown in figure 18 S (see SI). It is observed that the crystallite sizes and the lattice parameter decrease with increasing Al-content. The decrease of the unit cell parameter is in good agreement with the smaller radius of Al^{3+} ions (0.53 Å at coordination 4 and 0.675 Å), than Fe^{3+} ions (0.63 at coordination 4 and 0.785 in high spin configuration at coordination 6) and Ni^{2+} (0.69 at coordination 4 and 0.83 at coordination 6). Despite the low quality of the XRD data, aluminum occupancies were tentatively refined for compositions x = 0.5 and x = 1.5, respectively. In both cases, the tendency was an equal repartition of Al^{3+} ions in both sites.

Ni-Al ferrite powders were further investigated using laser Raman spectroscopy in order to ascertain the structure of the catalysts. The Raman spectra are given in Figs. 3 and 4 for samples prepared from chloride salts and nitrates precursors, respectively. As observed by XRD,

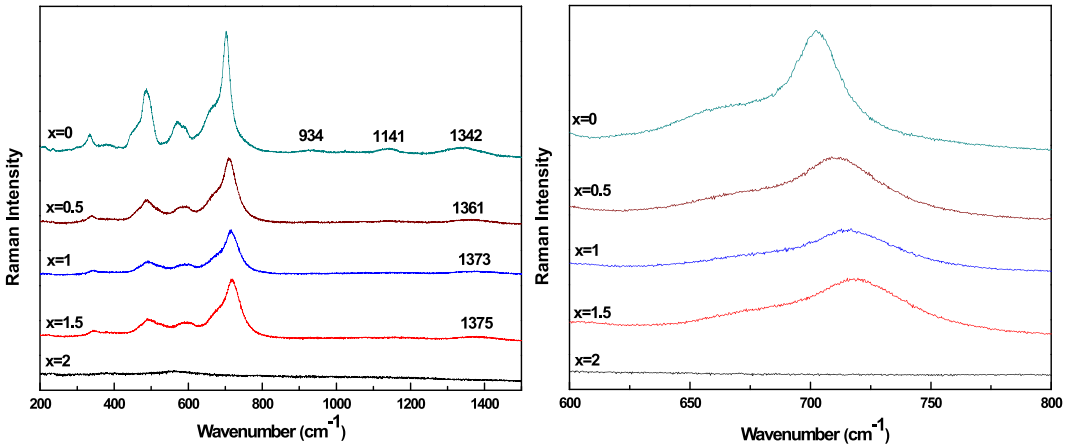

Fig. 3. Raman spectra of $NiAl_xFe_{2-x}O_4$ (x = 0; 0.5; 1; 1.5 and 2) spinel catalysts prepared from chloride salts, figure on the left is a zoom of the main peak at ~700 cm^{-1}.

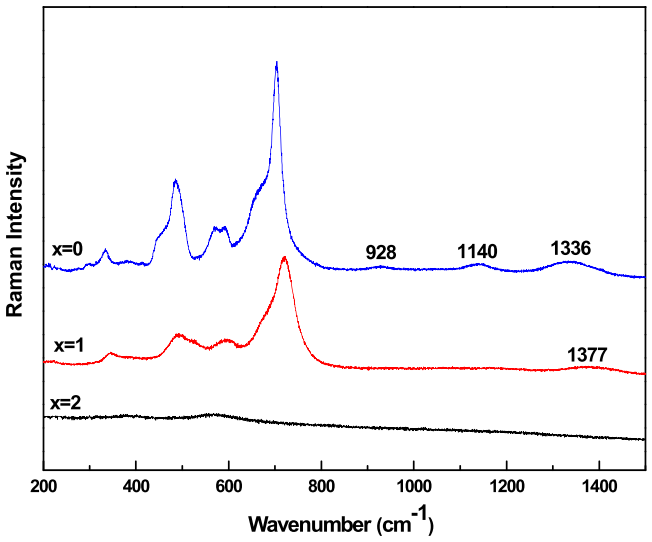

Fig. 4. Raman spectra of $NiAl_xFe_{2-x}O_4$ (x = 0; 1 and 2) spinel catalysts prepared from nitrate salts.

a shift towards higher frequencies of the characteristic peak of the spinel structure located at ~700 cm^{-1} confirms the incorporation of Al-species in the structure and the formation of a solid solution.

The Raman spectra of $NiFe_2O_4$ catalysts (x = 0) showed the five fundamental internal modes $A_{1\,g}+E_g+3\,T_{2\,g}$ in agreement with the rule selection for AB_2O_4 inverse spinel structure with $Fd\bar{3}m$ space group [25–27]. The corresponding wavenumbers are illustrated in Table 3, they are in good agreement with the literature [25–27]. The intense band with shoulders observed at ~704 cm^{-1} correspond to stretching motion of tetrahedral FeO_4 group and the other bands located at lower wavenumbers are attributed to the FeO_6 entity. The latter ones overlap with both the angular motion vibrations of the tetrahedral FeO species and lattice modes [28,29]. However, it should be noted that even if according to XRD study, $NiFe_2O_4$ (x = 0) catalyst was thought to be a single phase, Raman spectroscopy revealed extra weak peaks toward ~934 cm^{-1} (for $NiFe_2O_4$ (Cl^-)) and ~928 cm^{-1} for ($NiFe_2O_4$ (NO_3^-)) which could be assigned to NiO oxide [30] probably present either in a too small amount to be detected by XRD or in an amorphous state. In addition, the spectra show also two bands with low intensity at ~1141 and ~1342 cm^{-1} for $NiFe_2O_4$ (Cl^-) and ~1140 and ~1336 cm^{-1} for $NiFe_2O_4$ (NO_3^-) which can be attributed to Fe_2O_3 phase [31,32] in good agreement with what was observed by XPS. Indeed, in the preparation of $NiFe_2O_4$ spinel, the formation of small amount of iron oxide such as α-Fe_2O_3 and γ-Fe_2O_3 is often observed, these oxides have common lines with $NiFe_2O_4$ structure in XRD patterns which leads to difficulty to distinguish them, more especially in case of traces, amorphous or nanosized particles.

The Raman spectra of mixed catalysts $NiAl_xFe_{2-x}O_4$ (x = 0.5, 1 and 1.5) exhibit similar spectral feature. As shown in Table 3, the bands shift towards higher wavenumber as Al-content increases. This is the fingerprint of the formation of solid solutions and then the substitution of Fe by Al. The increase of the wavenumber value can be assigned to higher frequency values of the AlO_6 and AlO_4 species [33]. In addition, the spectra displayed very weak bands toward ~1375 cm^{-1} (x = 0.5), ~1373 cm^{-1} (x = 1) and ~1361 cm^{-1} (x = 1.5) for the catalyst issued from (Cl^-) precursors, ~1336 cm^{-1} (x = 0) and ~1377 cm^{-1} (x = 1) for the catalysts prepared with nitrates salts. As for $NiFe_2O_4$ this result suggests the presence of γ-Fe_2O_3 [31,32] and is in agreement with the thermal analysis results. Moreover, no characteristic band of pure NiO could be detected in mixed formulations probably due to a decrease of nickel impurities with the substitution of Fe by Al species with the intensity loss of the Raman lines with aluminum content.

ATR infra-red spectra of $NiAl_xFe_{2-x}O_4$ (0 ≤x ≤ 2) spinel type oxides prepared from (Cl^-) precursors are shown in Fig. 5 and the band

Table 3
FTIR and LSR modes of $NiAl_xFe_{2-x}O_4$ (0 ≤x ≤ 2) spinel structures.

	FTIR modes		Raman modes				
	ν_1 (~400 cm^{-1})	ν_2 (~600 cm^{-1})	$T_{2\,g}$	E_g	$T_{2\,g}$	$T_{2\,g}$	$A_{1\,g}$
$NiFe_2O_4$ (Cl^-)	369	554	210	334	486	572	704
$NiAl_{0.5}Fe_{1.5}O_4$ (Cl^-)	376	561	213	344	491	594	718
$NiAlFeO_4$(Cl^-)	385	577	210	344	491	591	714
$NiAl_{1.5}Fe_{0.5}O_4$ (Cl^-)	391	608	210	340	488	587	711
$NiAl_2O_4$ (Cl^-)	433	710	–	380	–	561	–
$NiFe_2O_4$ (NO_3^-)	–	–	213	334	486	571	704
$NiAlFeO_4$ (NO_3^-)	–	–	215	346	494	595	720

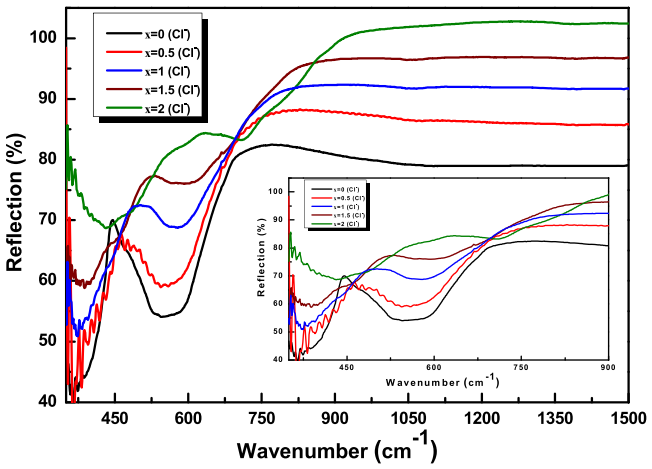

Fig. 5. ATR spectra measured at room temperature of $NiAl_xFe_{2-x}O_4$ ($0 \leq x \leq 2$) spinel type oxides prepared from chlorides anions.

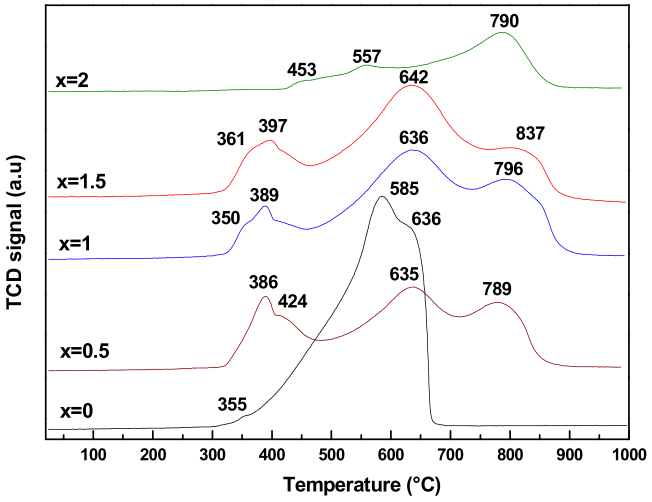

Fig. 6. H_2-TPR profiles of $NiAl_xFe_{2-x}O_4$ ($0 \leq x \leq 2$) spinel catalysts prepared from chloride salts.

positions are listed in Table 3 as function of Al-content. The obtained results of catalysts depict the presence of two prominent absorption bands located at ~400 (ν_1) and ~600 cm^{-1} (ν_2) thus characterizing the formation of spinel structure having two sublattices: octahedral [A] and tetrahedral [B] sites [34], as expected. The first band (~400 cm^{-1}) is assigned to octahedral group while the second (~ 600 cm^{-1}) is attributed to the stretching vibration mode of metal-oxygen at tetrahedral position. The intensity of these two absorption bands increases with the amount of Al-species ($0.5 \leq x \leq 2$) (Fig. 5). Interestingly the wavenumbers of each band increase with the amount of Al-species, in good agreement with aluminum substitution in both sites. The broad bands at ~ 3430 and ~1645 cm^{-1} observed only for x = 0 ($NiAl_2O_4$) are assigned to -OH stretching vibrational modes and bending vibrational mode of absorbed H_2O molecules, respectively. This band detected only in $NiAl_2O_4$ case can be explained by the high S_{BET} (149 m^2/g) of this catalyst which favors a quick adsorption of water from the atmosphere.

3.4. Reducibility measurements

The reduction behavior of $NiAl_xFe_{2-x}O_4$ ($0 \leq x \leq 2$) spinel type oxides prepared from (Cl^-) and (NO_3^-) precursors and calcined at 800 °C was studied by H_2-TPR, in situ XRD and TGA at variable temperature under H_2 atmosphere. The recorded H_2-TPR profiles are illustrated in

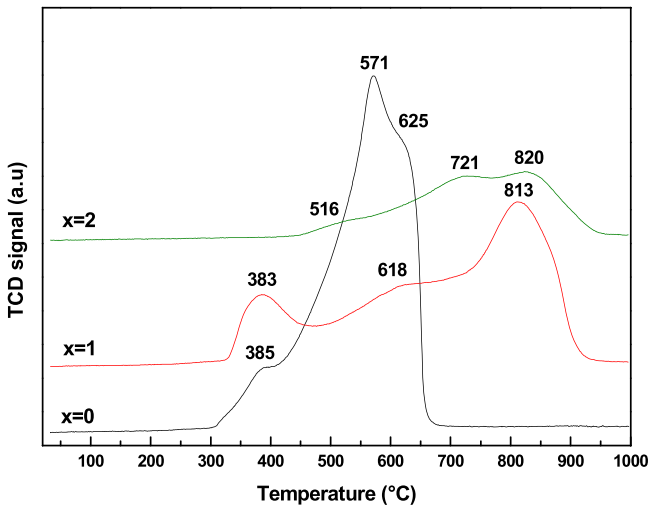

Fig. 7. H_2-TPR profiles of $NiAl_xFe_{2-x}O_4$ (x = 0; 1; 2) spinel catalysts prepared from nitrate salts.

Figs. 6 and 7. For all x values and whatever the used precursor (Cl^-) or (NO_3^-), the reduction process takes place mainly in three stages which differ by the reduction temperature. The amount of consumed H_2 does not depend on the used precursors but decreases as Al-content increases. It is worth noting that the small amount of consumed H_2 observed for the binary aluminate spinel x = 2 ~ 5.6 mmol/g (Figure 19 S, see SI) indicates that incorporation of Al-species makes the reduction of Ni^{2+} and Fe^{3+} species ($0 \leq x \leq 1.5$) more difficult. For these compounds, the reduction takes place at higher temperature. In inverse spinel structure, M^{3+} species occupy both crystallographic positions: 50% of the ions in the octahedral-[Oh] position and 50% in tetrahedral-[Td] sites. Thus, these species can undergo a reduction at different temperatures and hence, the M^{3+} species in [Td] sites would be reduced at lower temperatures compared to M^{3+} in [Oh] sites. In addition, the surface species are also reduced at lower temperatures compared to species in the bulk. The H_2-TPR profile shape of $NiFe_2O_4$ (synthetized from either (Cl^-) or (NO_3^-)) is totally different from the other formulations containing Al-species with a much higher consumed H_2 amount (~18 mmol/g) (Figure 19 S, see SI) and a reduction occurring at lower temperature (Figs. 6 and 7). The first peak (~355–385 °C) observed on H_2-TPR profile for x = 0 is attributed to the partial or total reduction of Fe^{3+} species in the [Td] sites of the spinel structure and those located on surface (Fe:Ni=5.7) at the expense of Fe_2O_3 ($Fe_2O_3 + 3\,H_2 \rightarrow 2Fe + 3\,H_2O$) in accordance with XPS and Raman experiments. Note that since the reduction temperature of Ni species is low, we cannot exclude that part of Ni contained in the spinel structure can be reduced in parallel with Fe^{3+}. The second peak located at ~585 °C (Cl^-) and at ~571 °C (NO_3^-) is assigned to the total reduction of Ni^{2+} species present in ferrite spinel structure and the third to the reduction of Fe^{3+} in [Oh] position of $NiFe_2O_4$ structure. The ternary catalysts issued from chlorides salts present similar H_2-TPR profiles but with reduction peaks shifted towards higher temperature, due to Al-content. The first peaks associated to shoulders at ~389–397 °C are assigned to the reduction of NiO to Ni° nanoparticles, whereas the other peaks are ascribed to the reduction of Ni^{2+} and Fe^{3+} of spinel. The system x = 1 (NO_3^-) (Fig. 7) presents neat reduction peaks compared to its Cl^- counterpart (Fig. 6) explaining an easier reduction for the nitrate-issued compound, in good agreement with the smaller crystallite size of NiO (14.8 nm against 92.6 nm for x = 1 (Cl^-)) (Table 2). As for the specific surface areas, the precursors have a huge influence on the reduction temperature for the aluminate spinel $NiAl_2O_4$. Thus, the reduction temperatures of the systems derived from (NO_3^-), which presented the best $S_{B.E.T}$ = 149 m^2/g, are higher compared to those prepared from (Cl^-) salts ($S_{B.E.T}$ =101 m^2/g) (Figs. 6 and 7) suggesting a strong interaction between Ni and Al-species in the

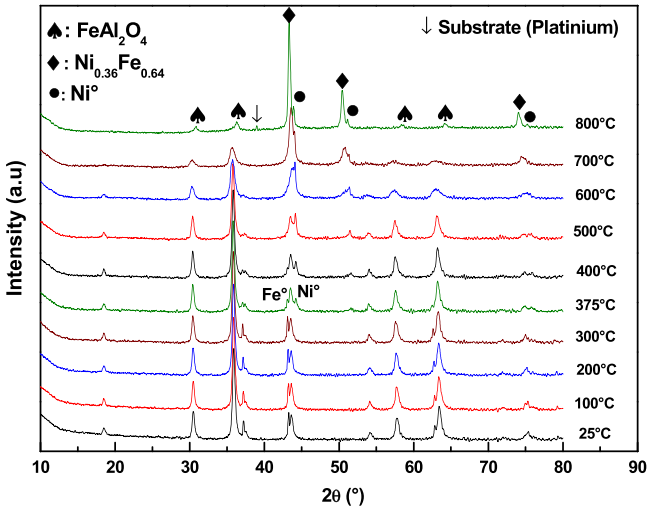

Fig. 8. HTXRD patterns of $NiAlFeO_4$ (Cl^-) catalyst during reduction by hydrogen (3% H_2 in N_2) up to 800 °C.

presence of (NO_3^-) anions. On TPR profiles of these formulations, only the reduction of the Ni species is observed because it is well-known that Al^{3+} cannot be reduced at temperatures lower than 1000 °C [35]. The first two peaks located at (~453–557 °C)(Cl^-) and (~516–721 °C)(NO_3^-) were attributed to the reduction of some free NiO species into Ni metallic. The broad peak, with a maximum at ~790 °C (Cl^-) and at ~820 °C (NO_3^-), corresponds to the reduction of Ni^{2+} engaged in the $NiAl_2O_4$ structure.

The reduction of $NiAlFeO_4$ sample prepared from (Cl^-) salts was also followed by high temperature X-Ray Diffraction under flowing hydrogen (Fig. 8). The results are in accordance with H_2-TPR measurements. The catalyst was stable up to 375 °C. In the temperature range 375–450 °C, the reduction of both species Ni^{2+} and Fe^{3+} takes place simultaneously: (i) NiO reduction ($NiO + H_2 \rightarrow Ni + H_2O$) was observed by the appearance of the cubic face centered (cfc) metallic Ni (*PDF: 03–065–2865*) and (ii) α-Fe ($NiFeAlO_4 + H_2 \rightarrow Fe_2O_3 + H_2O$ then $Fe_2O_3 + H_2 \rightarrow Fe + H_2O$), (*JCPDF 03–65–4899*) was formed. Ni and α-Fe were stable up to 600 °C and then form a Ni-Fe alloy (*PDF: 00–047–1405*), $FeAl_2O_4$ spinel oxide (*PDF: 01–082–1580*) and metallic Ni- (*PDF: 03–065–2865*). Several authors proposed the formation of FeO, Fe_2O_3 or Fe_3O_4 [36–38] as intermediates in the reduction mechanism of the spinel phase. Here, none of these phases were observed nor Al_2O_3, likely because they are not easy to detect due to their low content in the sample and/or their small crystallite size and/or probably because $FeAl_2O_4$ spinel phase and Ni-Fe alloys are formed after iron and nickel metallic formation at the expense of Fe_2O_3 and Al_2O_3, respectively. Note however that we cannot exclude the possibility that $FeAl_2O_4$ oxide and Ni-Fe alloy could come directly from the collapse of the spinel phase under H_2 flow. After return back to room temperature, a mixture of (i) nickel-iron alloy, (ii) aluminum-iron spinel phase and (iii) nickel-metal, which can be slightly alloyed, was evidenced. The formation of Ni-Fe alloy and $FeAl_2O_4$ spinel oxide detected by H_2-HTXRD around ~600 °C coincides with the maximum consumption of H_2 (~636 °C) on H_2-TPR profile of $NiAlFeO_4$ (Cl^-) (Fig. 6). Based on H_2-HTXRD results, the peaks at low temperatures (~350–389 °C) in H_2-TPR profile of $NiAlFeO_4$ (Cl^-) catalyst (Fig. 6) could be attributed to the simultaneous reduction of (i) Ni^{2+} species in free NiO oxide and (ii) of Fe^{3+} species engaged in spinel structure. However, the peaks observed at ~636 °C and 797 °C are related to the spinel structure reduction.

In order to give additional information on the reducibility properties and on the amount of reduced species present in catalyst, TGA under H_2 was carried out on both binary spinels issued from chloride precursors $NiFe_2O_4$ and $NiAl_2O_4$ (Fig. 9). The analysis was carried out at 400 °C for 5 h under H_2 atmosphere on samples previously calcined at 800 °C. Similarly, as H_2-TPR, a different behavior between $NiFe_2O_4$ and $NiAl_2O_4$ is observed for TGA analysis under H_2. For the $NiAl_2O_4$ (Cl^-) formulation, which according to XRD data is composed of 90% of spinel phase and 10% of NiO, a weight loss of 4.32% has been recorded during 5 h of treatment. Assuming that all Ni species of NiO oxide and those of spinel structure at tetrahedral sites are reduced, the theoretical weight loss of oxygen related to NiO and $NiAl_2O_4$ are 2.14% and 1.3%, respectively. This value is close to the measured one, explaining that all the nickel (II) present in the formulation x = 1 (in both NiO and spinel-type oxides) are reduced to metallic Ni(0) (Fig. 9). In contrast, for the pure ferrite spinel $NiFe_2O_4$ (Cl^-) formulation, the recorded thermogram (Fig. 8(a)) shows a much higher 26.5% weight loss after 3 h of treatment, value in good accordance with the theoretical weight loss of oxygen (27.3%) expected for the full reduction of the $NiFe_2O_4$ spinel structure. Interestingly, the reduction process starts before the plateau at 400 °C which means the iron spinel is easier to reduce than the aluminum one. This is in good agreement with the H_2-HTXRD carried out on the mixed Al-Fe spinel. The more iron in the sample, the more reducible it is and, in contrast, the more aluminum in the sample the more stable against reduction it is.

3.5. Catalytic properties in dry reforming of methane

The $NiAl_xFe_{2-x}O_4$ catalysts prepared from (Cl^-) and (NO_3^-) and calcined at 800 °C under air flow were tested on the dry reforming reaction of methane ($CO_2 + CH_4 \leftrightarrow 2CO + 2\,H_2$, $\Delta H°_{298}$ =247 kJ/mol). Figs. 10, 11 and 12 show the catalytic performances without any previous treatment (CH_4 conversion, CO_2 conversion, H_2/CO ratio and X_{CH4}/X_{CO2} ratio) in the temperature range 650–800 °C. The equilibrium

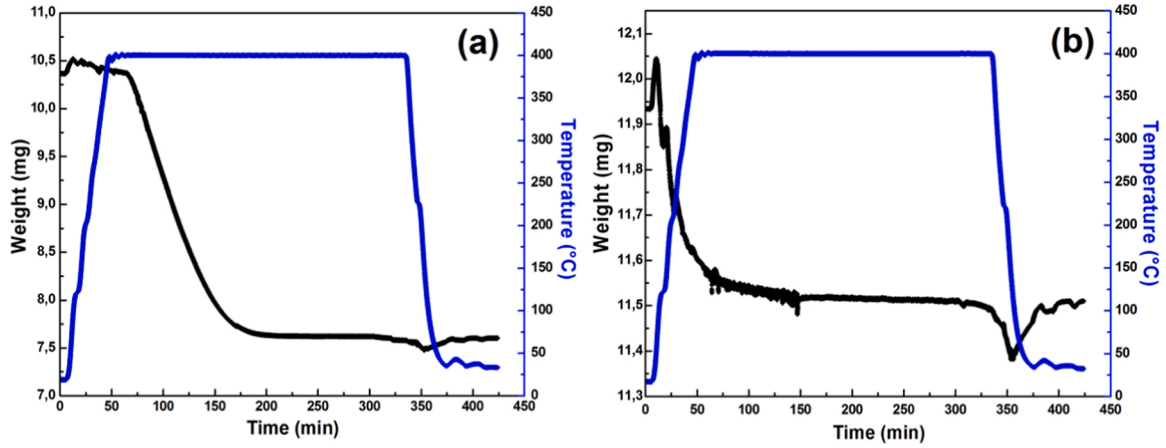

Fig. 9. TGA thermogram of (a) $NiAl_2O_4$ (Cl^-) and (b) $NiFe_2O_4$(Cl^-) catalysts during reduction by hydrogen (5% H_2 in Ar) up to 400 °C.

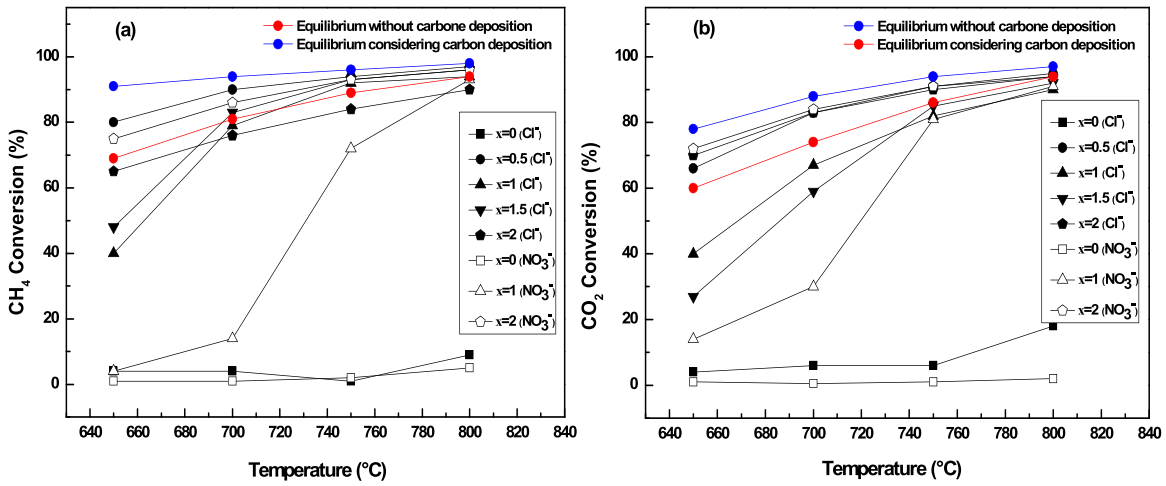

Fig. 10. CH_4 (a) and CO_2 (b) conversions obtained on the fresh $NiAl_xFe_{2-x}O_4$ spinel catalysts co-precipitated from nitrate and chloride salts ($0 \leq x \leq 2$) (CH_4 =20%; CO_2 =20%; 200 mg; F=100 mL/min).

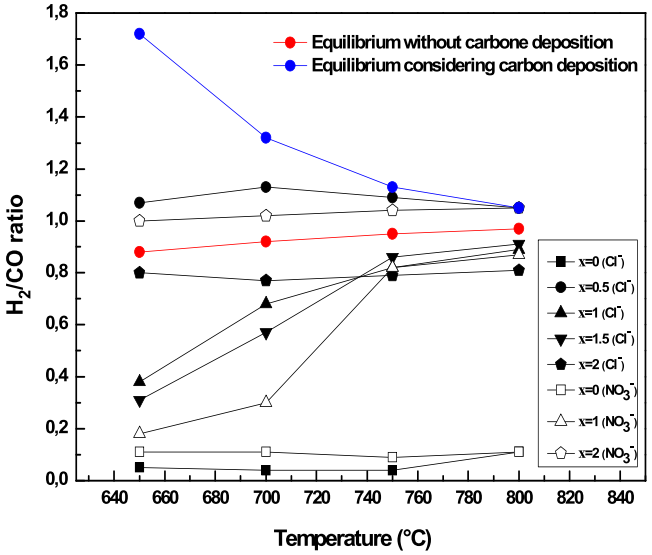

Fig. 11. H_2/CO ratios obtained on the fresh $NiAl_xFe_{2-x}O_4$ spinel catalysts co-precipitated from nitrate and chloride salts ($0 \leq x \leq 2$) (CH_4 =20%; CO_2 =20%; 200 mg; F=100 mL/min).

conversions and H_2/CO ratio are also reported in Figs. 10 and 11 taking in consideration all possible reaction products (including carbon deposition) or only DRM and RWGS reactions (without carbon deposition).

All tested catalysts are catalytically active in dry reforming reaction except the formulations x = 0, which presents a poor activity even at high temperature, despite a significant reduction capacity difference expected after the (H_2-TPR) of $NiFe_2O_4$ compared to the formulations containing Al-species. This low activity of $NiFe_2O_4$ without any pretreatment is not surprising, and has already been observed on ferrite spinels prepared by other routes such as coprecipitation/CO_3^{-} [21], hydrothermal [21] and sol-gel [9] methods.

On the other hand, the incorporation of aluminum in ferrite spinel structures has a spectacular effect on the catalytic activity in dry reforming of methane. In the temperature range 650–750 °C, conversions varied to finally stabilize at ~90–96% i.e. near to thermodynamic equilibrium values, when the temperature increases up to 800 °C. For x = 1, the sample issued from chloride salts shows higher conversion than nitrate sample: $X(\%)_{CH4}(x = 1(Cl^-))$~41% against $X(\%)_{CH4}(x = 1(NO_3^-))$~4% at 650 °C and $X(\%)_{CH4}(x = 1(Cl^-))$~92% against $X(\%)_{CO2}(x = 1(NO_3^-))$~72% at 750 °C while at 800 °C, the same conversions are observed whatever the precursors. Again, this is indicative that thermodynamic equilibrium is reached at such high temperature. In contrast, for the binary aluminate spinel (x = 2) and in all the temperature range $X(\%)_{CH4}(NO_3^-)$ is ~10% higher than $X(\%)_{CH4}(Cl^-)$ (Fig. 10). Whatever the precursor, at Al-content $x \geq 0.5$, CO_2-conversions are lower than CH_4-conversions, which can be attributed to several parameters (i) a low contribution of WRGS reaction ($CO_2 + H_2 \leftrightarrow CO + H_2O$), (ii) some methane decomposition as a secondary reaction ($CH_4 \rightarrow C + 2\,H_2$ methane cracking, $\Delta G(800\,°C) = -33.95$Kj/mol) [39] and (iii) dry reforming reaction being the main occurring reaction which is also confirmed by the fact that the molar H_2/CO ratio is < 1 (Fig. 11). The H_2/CO ratios of Al-Fe mixed oxides ($0.5 \leq x \leq 1.5$) decreases when the amount of Al increases, indicating its important role in mitigating side reactions. For the iron-rich formulation (x = 0.5), a slight difference between H_2/CO experimental and theoretical is observed ($\Delta_{H2/CO}$) ~0.05–0.13, probably due to the migration of Fe^{3+} species from the bulk on the surface of $NiAl_{0.5}Fe_{1.5}O_4$ sample (see XPS). At x = 1 and 1.5 values, the Al-content influence is significant on H_2/CO between 650 and 700 °C but becomes negligible at high temperature. The H_2/CO ratio of binary aluminate spinel $NiAl_2O_4$ depends on the precursor but is stable throughout the temperature range studied (650–800 °C), with ratio close to one for nitrates and ~0.8 for chloride ones.

To summarize, the unreduced ferrite spinel catalysts $NiFe_2O_4$ (x = 0), whatever the precursor, exhibit low activity and very low H_2/CO ratios compared to catalysts of the same structural type, $NiAl_2O_4$ (x = 2) or ternary compounds $NiAl_xFe_{2-x}O_4$ ($0.5 \leq x \leq 1.5$). Their activity is also lower than binary $NiCr_2O_4$, $NiMn_2O_4$ activity [4]. The used precursors (Cl^-) or (NO_3^-) affects significantly the bulk and surface properties and consequently the catalytic activity of catalysts containing Al-species. For $NiAl_xFe_{2-x}O_4$ ($0.5 \leq x \leq 1.5$), chlorides salts show the higher initial activity compared to nitrates precursors. In contrast, for binary aluminate spinel $NiAl_2O_4$ who has the best catalytic activity in CH_4/CO_2 reaction (H_2/CO~1) throughout the studied temperatures range, the nitrate sample shows the best performances in all temperature range. Nichio et al. [40] reported that the use of nitrates and acetylacetonate as precursors for Ni based catalysts has no effect on the catalytic activity in partial oxidation of methane but Takayasu et al. [41] and Boitiaux et al. [42] showed the opposite effect. They reported that the use of acetylacetonate precursor led to a high dispersion of active site and good catalytic activity in dry reforming of methane. While, Ruckenstein et al. [43] showed that lanthanum supported Ni catalysts prepared from nitrates salts had an important initial activity but low stability in dry reforming of methane, in contrast, the same catalyst prepared from chloride precursors had high stability. In term of

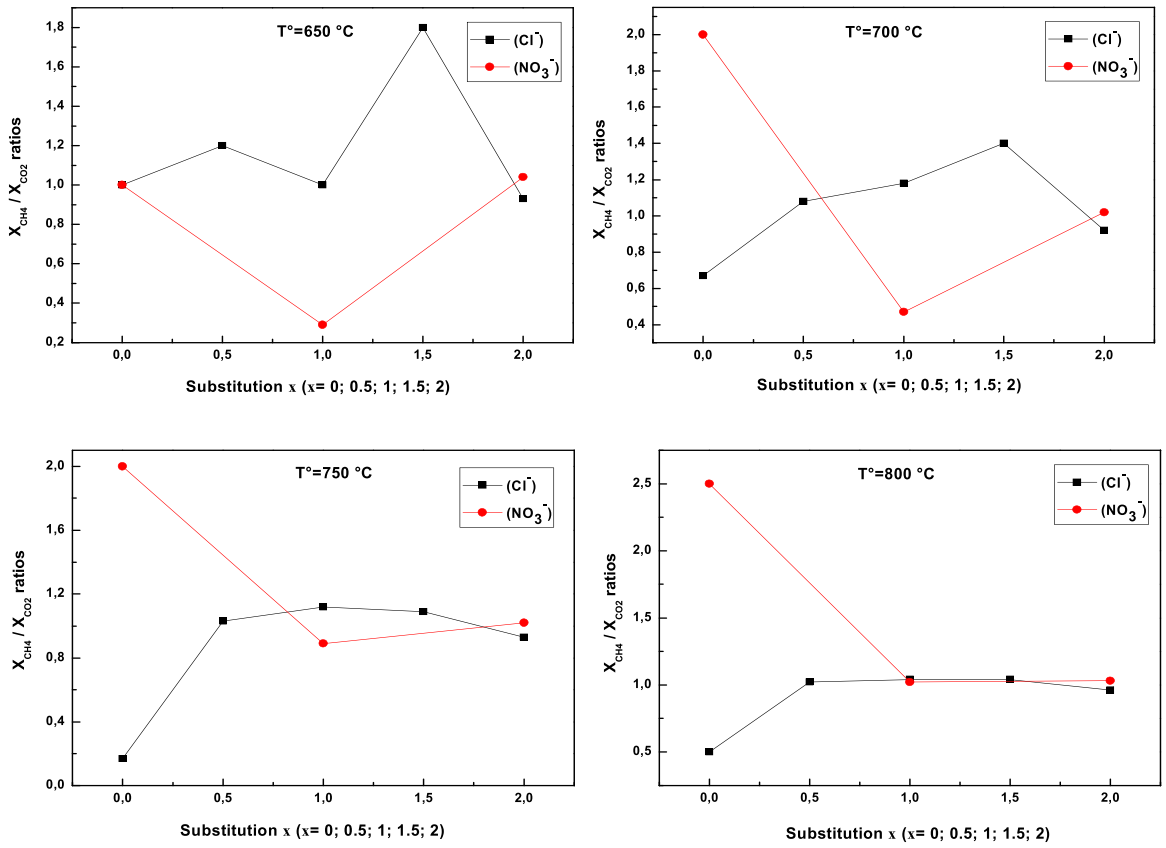

Fig. 12. X_{CH4}/X_{CO2} ratios at 650, 700, 750 and 800 °C obtained on the fresh $NiAl_xFe_{2-x}O_4$ spinel catalysts co-precipitated from nitrate and chloride salts ($0 \leq x \leq 2$) (CH_4 =20%; CO_2 =20%; 200 mg; F=100 mL/min).

comparison, in our operating conditions, the obtained results in dry reforming of methane without any previous treatment are very promising compared to the literature. Martinez et al. [44] found after reduction under H_2 flow of Ni-Al catalyst, CH_4 and CO_2 conversions not exceeding 40% at 700 °C.

As reported in this paper and also published in our previous works [9,20], we attribute the low activity of ferrite spinel oxides $NiFe_2O_4$ to the absence of active Ni-metallic phase, related to the formation of Ni-Fe alloy at the expense of Ni° and Fe° reduced species under reaction mixture, or to the collapse of the spinel phase under a reducing atmosphere. Whatever the precursor, the H_2/CO ratio values is not exceeding ~0.11 (Fig. 11), a very low value compared to the theoretical unit value, implying the participation of side reactions. such as (i) $CO + 3\ H_2 \rightarrow CH_4 + H_2O$, (ii) $CO_2 + 4\ H_2 \rightarrow CH_4 + 2\ H_2O$ and/or (iii) RWGS ($CO_2 + H_2 \leftrightarrow CO + H_2O$). The contribution of the first two reactions (i) and (ii) can be excluded for thermodynamic reasons ($\Delta G<0$ if $T < 500$ °C for both reactions, at 800 °C, $\Delta G(i) \sim +55.41$Kj/mol and $\Delta G(ii) \sim +55.98$Kj/mol [39]). The contribution of RWGS reaction which tends to decrease the production of H_2 seems thus the most likely ($\Delta G \sim 0.5$ Kj/mol), leading to a reoxidation of the active sites (Ni°) by H_2O vapor formed during the catalytic test. One of the possible explanations is the degradation of the active surface due to a joint effect of the temperature and the reaction medium which results in an insufficient presence of active sites on the surface. This could be due to either an increase size of the metallic particles by sintering, that would cause a decrease of the active surface or to a migration of iron species (from the bulk to the surface) that would mask the active sites, or even a reoxidation of the active metallic phase due to the magnitude of RWGS reaction. The low activity observed on spinel ferrites (x = 0) can be correlated by its (i) textural characteristics such as, a low $S_{B.E.T} < 10\ m^2/g$, a low amount of lattice oxygen on the surface and presence of excess Fe^{3+} species on the $NiFe_2O_4$-surface which favored RWGS reaction (XPS data, Table 1), (ii) structural properties showing the presence of Fe_2O_3 phase and (iii) its reducibility as observed by TGA under H_2 (Fig. 9). It was indeed noticed that a considerable amount of Ni° and Fe° reduced species (~26%) is lost and transformed into an inactive Ni-Fe alloy, as shown by in-situ HTXRD under flowing H_2. Anyway, it might be inferred that the heating to 800 °C during catalysis could have destroyed (at least on the surface) the spinel phase to directly deliver the Ni-Fe alloy.

Interestingly, the substitution of Fe by Al plays a primordial role in catalytic activity in dry reforming reaction; it increases significantly the catalytic performances which confirms the existing synergetic effect between Al and Fe-species that promotes the activation of the samples. The H_2/CO ratio is similar or lower compared to the nominal reaction composition for all formulations containing Al-species, which also explains the negligible contribution of RWGS reaction. We propose, based on HTXRD under H_2 for $NiAlFeO_4$ (Cl^-) sample (Fig. 8), that insertion of aluminum would stabilize Ni activity, via the formation of $FeAl_2O_4$ spinel phase, that consumes iron, preventing the formation of detrimental Ni-Fe alloy or metallic iron. It is well known that RWGS is favored in the presence of iron species, then the in-situ formation of such $FeAl_2O_4$ which disadvantages RWGS would thus liberate the active sites of Ni°. Unlike $NiFe_2O_4$ which showed a loss of reduced species in ATG analysis under H_2, the aluminate $NiAl_2O_4$ sample keeps the amount of reduced species throughout the whole reaction and since the reduced Ni-species has no affinity with Al-species, it could explain the stabilizing effect of aluminum and the excellent catalytic performances. In addition, the catalytic activity of $NiAl_2O_4$ is well correlated with the higher specific surface area (149 m^2/g), the lower crystallites size (7 nm) and the localization of Ni^{2+} species at the surface (Table 1).

After reaction, the catalysts were heated in air at 700 °C for 30 min in order to detect the formation of carbon oxides that would have come from coking according to the Boudouard ($2CO \rightarrow C+CO_2$) and methane cracking reactions ($CH_4 \rightarrow C + 2\ H_2$). The obtained quantifications of

Table 4
The amount (% ± 1) of coke deposit over the catalysts after CH_4/CO_2 reaction.

T (°C)	x = 0 (Cl^-)	x = 0.5 (Cl^-)	x = 1 (Cl^-)	x = 1.5 (Cl^-)	x = 2 (Cl^-)	x = 0 (NO_3^-)	x = 1 (NO_3^-)	x = 2 (NO_3^-)
650	45	20	< 2	< 1.5	7	–	–	7
700	20	20	4	< 2	3.7	–	–	5
750	< 2	11	5	7	3.6	–	–	4
800	< 1	4	5	6	3	–	–	4

coke deposit are depicted in the Table 4. Excepted for both x = 0 (Cl-) and x = 0.5 (Cl-) samples, the coke deposit values are note influenced by the reaction temperature. In all reaction temperatures range, the recorded amount of coke deposit not exceeding 7% whatever the used precursor that explain a good resistance against coke formation. This resistance can be interpreted by the presence of $FeAl_2O_4$ spinel phase which plays a crucial role as catalytic precursor in the in-situ production of Ni° nanoparticles, highly dispersed and less prone to coke formation in spite of the severe reaction conditions. Both x = 0 (Cl^-) and x = 0.5 (Cl^-) show a high amount at low reaction temperature but this quantity decreases and become as the same values of other catalysts at higher reaction temperature (At 800 °C). The low amount of carbon deposit at higher reaction temperatures all catalysts can be explained by the decrease of amount of Ni metallic species which responsible to the coke formation or by the change of the behavior of the catalytic surface.

4. Conclusion

The insertion of Al-species and the nature of salts, chloride or nitrate, used as precursors for the synthesis of Fe-Ni spinel oxides affect significantly the bulk, the surface composition and the reducibility properties as well as their activity in dry reforming of methane to syngas production.

The catalytic properties in the dry reforming of methane by carbon dioxide studied with the pristine (unreduced) spinel samples of binary ($NiAl_2O_4$) and ternary aluminate spinels ($NiAl_xFe_{2-x}O_4$, x ‡ 0) are very promising. In contrast, the very poor activity observed in pure iron $NiFe_2O_4$ case, (x = 0) can be explained by the loss of Ni-metal during catalytic process, due to the formation of Ni-Fe alloy favoring RWGS reaction. The formation of this alloy is favored once Fe° and Ni° are formed. The insertion of a small amount of Al-species (x = 0.5) improves the activity of the catalyst by the creation of a very stable $FeAl_2O_4$ compounds that inhibits the agglomeration of Ni-metallic species. In addition, the mixed formulations (x = 1) synthesized from (Cl^-) are more active compared to those prepared from (NO_3^-) at low reaction temperatures, but this behavior attenuates at high temperature. Under our operating conditions and without any previous treatment, the binary aluminate spinel issued from nitrates salts is the most active in dry reforming of methane, the activity being related to several synergetic parameters such as the higher specific surface area, the smaller crystallites size, the presence of Ni^{2+} species on the surface and to their stability, the dispersion of Ni-metallic insured by alumina oxide which led to a good orientation of the reaction by minimizing the effects of side reactions such as RWGS.

Finally, catalytic experiments of dry reforming of methane show that nickel aluminate ferrite oxides are suitable catalysts under the conditions we used. The results presented in this study show the importance of the incorporation of Al-species as well as the importance of in-situ formed intermediate phases occurring during the reaction.

Declaration of Competing Interest

The authors declare that they have no known competing financial interests or personal relationships that could have appeared to influence the work reported in this paper.

Data Availability

No data was used for the research described in the article.

Acknowledgements

The Fonds Européen de Développement Régional (FEDER), CNRS, Région Hauts-de-France, Chevreul Institute (FR 2638) and the French Ministère de l'Education Nationale, de l'Enseignement Supérieur et de la Recherche are acknowledged for funding characterization facilities (XPS/LEIS/ToF-SIMS spectrometers, X-Ray diffractometers and SEM instruments). The authors are also grateful to Olivier Gardol, Laurence Burylo, Maxence Vandewalle and Nora Djelal for the technical assistance.

Appendix A. Supporting information

Supplementary data associated with this article can be found in the online version at doi:10.1016/j.jcou.2022.102319.

References

[1] X. Zhang, C. Yang, Y. Zhang, Y. Xu, S. Shang, Y. Yin, Ni-Co catalyst derived from layered double hydroxides for dry reforming of methane, Int. J. Hydrog. Energy 40 (2015) 16115–16126, https://doi.org/10.1016/j.ijhydene.2015.09.150.
[2] K. Mette, S. Kühl, H. Düdder, K. Kähler, A. Tarasov, M. Muhler, M. Behrens, Stable performance of Ni catalysts in the dry reforming of methane at high temperatures for the efficient conversion of CO_2 into syngas, ChemCatChem 6 (2014) 100–104, https://doi.org/10.1002/cctc.201300699.
[3] J.L. Ewbank, L. Kovarik, F.Z. Diallo, C. Sievers, Effect of metal support interactions in Ni/Al_2O_3 catalysts with low metal loading for methane dry reforming, Appl. Catal., A. 494 (2015) 57–67, https://doi.org/10.1016/j.apcata.2015.01.029.
[4] K. Rouibah, A. Barama, R. Benrabaa, J. Guerrero-Caballero, T. Kane, R.N. Vannier, A. Rubbens, A. Löfberg, Dry reforming of methane on nickel-chrome, nickel-cobalt and nickel-manganese catalysts, Int. J. Hydrog. Energy 42 (50) (2017) 29725–29734, https://doi.org/10.1016/j.ijhydene.2017.10.049.
[5] J.R. Rostrup-Nielsen, J.-H.Bak Hansen, CO_2 reforming of methane over transition metals, J. Catal. 144 (1993) 38–49, https://doi.org/10.1006/jcat.1993.1312.
[6] M.C.J. Bradford, M.A. Vannice, CO_2 Reforming of CH_4, Catal. Rev. Sci. Eng. 41 (1999) 1–42, https://doi.org/10.1081/CR-100101948.
[7] J.R. Rostrup-Nielsen, Production of synthesis gas, Catal. Today 18 (1993) 305–324, https://doi.org/10.1016/0920-5861(93)80059-A.
[8] S. Wang, G.Q. Lu, G.J. Millar, Carbon dioxide reforming of methane to produce synthesis gas over metal-supported catalysts: state of the art, Energy Fuels 10 (1996) 896–904, https://doi.org/10.1021/ef950227t.
[9] R. Benrabaa, A. Löfberg, A. Rubbens, E. Bordes-Richard, R.N. Vannier, A. Barama, Structure, reactivity and catalytic properties of nanoparticles of nickel ferrite in the dry reforming of methane, Catal. Today 203 (2013) 188–195, https://doi.org/10.1016/j.cattod.2012.06.002.
[10] F. Touahra, A. Rabahi, R. Chebout, A. Boudjemaa, D. Lerari, M. Sehailia, D. Halliche, K. Bachari, Enhanced catalytic behavior of surface dispersed nickel on $LaCuO_3$ perovskite in the production of syngas: An expedient approach to carbon resistance during CO_2 reforming of methane, Int. J. Hydrog. Energy 41 (2016) 2477–2486, https://doi.org/10.1016/j.ijhydene.2015.12.062.
[11] R. Benrabaa, A. Barama, H. Boukhlouf, J. Guerrero-Caballero, A. Rubbens, E. Bordes-Richard, A. Löfberg, R.N. Vannier, Physico-chemical properties and syngas production via dry reforming of methane over $NiAl_2O_4$ catalyst, Int. J. Hydrog. Energy 42 (2017) 12989–12996, https://doi.org/10.1016/j.ijhydene.2017.04.030.
[12] E. Ruckenstein, Y.H. Hu, Carbon dioxide reforming of methane over nickel/alkaline earth metal oxide catalysts, Appl. Catal., A. 133 (1995) 149–161, https://doi.org/10.1016/0926-860X(95)00201-4.
[13] O. Dewaele, G.F. Froment, TAP study of the mechanism and kinetics of the adsorption and combustion of methane on Ni/Al_2O_3 and NiO/Al_2O_3, J. Catal. 184 (1999) 499–513, https://doi.org/10.1006/jcat.1999.2473.
[14] J.A. Wang, X. Bokhimi, O. Novaro, T. Lopez, R. Gomez, Effects of the surface structure and experimental parameters on the isopropanol decomposition

catalyzed with sol-gel MgO, J. Mol. Catal. A: Chem. 145 (1999) 291–300, https://doi.org/10.1016/S1381-1169(99)00035-7.
[15] A. Gervasini, A. Auroux, Acidity and basicity of metal oxide surfaces II. Determination by catalytic decomposition of isopropanol, J. Catal. 131 (1991) 190–198, https://doi.org/10.1016/0021-9517(91)90335-2.
[16] A. Gervasini, A. Auroux, Microcalorimetric study of the acidity and basicity of metal oxide surfaces, J. Phys. Chem. 94 (1990) 6371–6379, https://doi.org/10.1021/j100379a041.
[17] P.N. Trikalitis, P.J. Pomonis, Catalytic activity and selectivity of perovskites $La_{1-x}Sr_xV^{3+}_{1-x}V^{4+}_xO_3$ for the transformation of isopropanol, Appl. Catal., A. 131 (1995) 309–322, https://doi.org/10.1016/0926-860X(95)00121-2.
[18] M.A. Aramendia, V. Borau, C. Jimenez, J.M. Marinas, A. Porras, F.G. Urbano, Magnesium oxides as basic catalysts for organic processes: study of the dehydrogenation-dehydration of 2-propanol, J. Catal. 161 (1996) 829–838, https://doi.org/10.1006/jcat.1996.0246.
[19] C. Arean, J.S.D. Vifiuela, Structural study of copper-nickel aluminate ($Cu_xNi_{1-x}A1_2O_4$) spinels, J. Solid State Chem. 60 (1985) l–5, https://doi.org/10.1016/0022-4596(85)90156-2.
[20] S. Kamali, K. Shih, B. Barbiellini, Y.J. Wang, S. Kaprzyk, M. Itou, A. Bansil, Y. Sakurai, Extracting the cation distributions in $NiFe_{2-x}Al_xO_4$ solid solutions using magnetic Compton scattering, J. Phys.: Condens. Matter 27 (2015) 456003–456008, https://doi.org/10.1088/0953-8984/27/45/456003.
[21] R. Benrabaa, H. Boukhlouf, A. Löfberg, A. Rubbens, R.N. Vannier, E. Bordes-Richard, Nickel ferrite spinel as catalyst precursor in the dry reforming of methane: synthesis, characterization and catalytic properties, J. Nat. Gas. Chem. 21 (2012) 595–604, https://doi.org/10.1016/S1003-9953(11)60408-8.
[22] J. Rodriguez-Carjaval, Recent advances in magnetic structure determination by neutron powder diffraction, Phys. B 192 (1993) 55–69, https://doi.org/10.1016/0921-4526(93)90108-I.
[23] ⟨http://www.xpsfitting.com/⟩.
[24] M.C. Biesingera, B.P. Payne, A.P. Grosvenor, L.W.M. Laua, A.R. Gerson, R.St.C. smart, resolving surface chemical states in XPS analysis of first row transition metals, oxides and hydroxides: Cr, Mn, Fe, Co and Ni, Appl. Surf. Sci. 257 (2011) 2717–2730, https://doi.org/10.1016/j.apsusc.2010.10.051.
[25] M.N. Iliev, D. Mazumdar, J.X. Ma, A. Gupta, F. Rigoto, J. Fonctcuberta, Monitoring B-site ordering and strain relaxation in $NiFe_2O_4$ epitaxial films by polarized Raman Spectroscopy, Phys. Rev. B83 (2011), 014108, https://doi.org/10.1103/PhysRevB.83.014108.
[26] V.G. Anju Ahlawat, V.R. Sathe, Raman and X-ray diffraction studies of superparamagnetic $NiFe_2O_4$ nanoparticles prepared by sol-gel auto-combustion method, J. Magn. Magn. Mater. 323 (2010) 2049–2054, https://doi.org/10.1103/PhysRevB.83.014108.
[27] D. Varshney, K. Verma, Substitutional effect on structural and dielectric properties of $Ni_{1-x}A_xFe_2O_4$ (A=Mg, Zn) mixed spinel ferrites, Mater. Chem. Phys. 140 (2013) 412–418, https://doi.org/10.1016/J.MATCHEMPHYS.2013.03.062.
[28] L. Wang, X. Li, J. Li, M. Liu, S. Xu, H. Li, Structural and electromagnetic properties of $NiAl_xFe_{2-x}O_4/SiO_2$ nanocomposite films deposited using a sol- gel spin coating method, J. Magn. Magn. Mater. 444 (2017) 193–197, https://doi.org/10.1016/j.jmmm.2017.08.025.
[29] J.A.C. de Paiva, M.P.F. Graça, J. Monteiro, M.A. Macedo, M.A. Valente, Spectroscopy studies of $NiFe_2O_4$ nanosized powders obtained using coconut water, J. Alloy. Compd. 485 (2009) 637–641, https://doi.org/10.1016/j.jallcom.2009.06.052.
[30] J.H. Kim, I.S. Hwan, Development of an in-situ Raman spectroscopic system for surface oxide films on metals and alloys in high temperature water, Nucl. Eng. Des. 235 (2005) 1029–1040, https://doi.org/10.1016/j.nucengdes.2004.12.002.
[31] L.C. Prinsloo, P. Colomban, J.D. Brink, I. Meiklejohn, A. Raman, spectroscopic study of the igneous rocks on Marion Island: a possible terrestrial analogue for the geology on Mars, J. Raman Spectrosc. 42 (2011) 626–632, https://doi.org/10.1002/jrs.2756.
[32] M. Giarola, G. Mariotto, D. Ajo, Micro-Raman investigations on inclusions of unusual habit in a commercial tanzanite gemstone, J. Raman Spectrosc. 43 (2012) 556–558, https://doi.org/10.1002/jrs.3059.
[33] J. Kreisel, G. Lucazeau, H. Vincent, Raman spectra and vibrational analysis of $BaFe_{12}O_{19}$ hexagonal ferrite, J. Solid State Chem. 137 (1998) 127–137, https://doi.org/10.1006/jssc.1997.7737.
[34] A.M. Shaikh, S.A. Jadhav, S.C. Watawe, B.K. Chougule, Infrared studies of some Li-Mg-Zn ferrites, Mater. Lett. 44 (2000) 192–196, https://doi.org/10.1016/S0167-577X(00)00025-2.
[35] S.P. de Lima, V. Vicentini, J.L.G. Fierro, M.C. Rangel, Effect of aluminum on the properties of lanthana-supported nickel catalysts, Catal. Today 133 (2008) 925–930, https://doi.org/10.1016/j.cattod.2007.12.065.
[36] L.J. Ma, L.S. Chen, S.Y. Chen, Effect of $NiFe_2O_4$ processing technology on decomposition of CO_2, Chin. J. Inorg. Chem. 23 (2007) 329–334.
[37] S. Kameoka, T. Tanabe, A.P. Tsai, Spinel $CuFe_2O_4$: a precursor for copper catalyst with high thermal stability and activity, Catal. Lett. 100 (2005) 89–93, https://doi.org/10.1007/s10562-004-3091-z.
[38] A. Khan, P. Chen, P. Boolchand, P.G. Smirniotis, Modified nano-crystalline ferrites for high-temperature WGS membrane reactor applications, J. Catal. 253 (2008) 91–104, https://doi.org/10.1016/j.jcat.2007.10.018.
[39] M.V. Sivaiah, S. Petit, M.F. Beaufort, D. Eyidi, J. Barrault, C. Batiot-Dupeyrat, S. Valange, Nickel based catalysts derived from hydrothermally synthesized 1:1 and 2:1 phyllosilicates as precursors for carbon dioxide reforming of methane, Microporous Mesoporous Mater. 140 (2011) 69–80, https://doi.org/10.1016/j.micromeso.2010.09.015.
[40] N. Nichio, M. Casella, O. Ferretti, M. González, C. Nicot, B. Moraweck, R. Frety, Partial oxidation of methane to synthesis gas. Behaviour of different Ni supported catalysts, Catal. Lett. 42 (1996) 65–72, https://doi.org/10.1007/BF00814468.
[41] O. Takayasu, C. Soman, Y. Takegahara, I. Matsuura, Deactivation of Ni-catalysts and its prevention by mechanically mixing an oxide for the formation reaction of $CO+H_2$ from CO_2+CH_4, Stud. Surf. Sci. Catal. 88 (1994) 281–288, https://doi.org/10.1016/S0167-2991(08)62751-2.
[42] J.P. Boitiaux, J. Cosyns, E. Robert, Additive effects in the selective hydrogenation of unsaturated hydrocarbons on platinum and rhodium catalysts: II. Influence of various compounds containing phosphorus, oxygen, sulphur and chlorine on the catalytic performance of platinum catalyst, Appl. Catal. 49 (1989) 235–246, https://doi.org/10.1016/S0166-9834(00)83020-1.
[43] E. Ruckenstein, Y.H. Hu, Interactions between Ni and La_2O_3in Ni/La_2O_3 catalysts prepared using different Ni precursors, J. Catal. 161 (1996) 55–61, https://doi.org/10.1006/jcat.1996.0161.
[44] R. Martinez, E. Romero, C. Guimon, R. Bilbao, CO_2 reforming of methane over coprecipitated Ni-Al catalysts modified with lanthanum, Appl. Catal. A. 274 (2004) 139–149, https://doi.org/10.1016/j.apcata.2004.06.017.

Rafik Benrabaa (Index h: 10, Index i10: 11), Professor, Director of the Physico-Chemistry of materials laboratory at Chadli BENDJEDID, EL-Taref University-Algeria. Obtained a doctorate from USTHB-Algiers in 2013 and promoted to Professor of University in 2020. My research activities focus on the development and characterization of supported (over natural materials) and unsupported catalytic materials applied for energy and the environment via catalytic and/or photocatalytic way. This present paper is the result of a collaboration between my laboratory and that of UCCS-Lille. My contribution in this article was on the preparation of the catalysts and their application in CH_4 +CO_2 reaction.

Pascal Roussel, CNRS Research Director, (293 publications, Index h: 41, Index i10: 179, source Google Scholar, march 2022), Senior researcher, Deputy-Director of the UCCS lab (more than 300 peoples), head of the X-ray facilities of Lille University (10 diffractometers). My research interests focus on the use of diffraction techniques (with electrons, neutrons or X-rays) to finely characterize structure and microstructure of materials, either on single crystals, powders or thin films, and their relationships to physical properties. My contribution in this article was on the XRD characterization.

Annick Rubbens, Professor at University of Lille, in charge of Raman scattering at the Unité de Catalyse et Chimie du Solid-axe Chimie du Solide. My contribution to this article was to carry out the investigations by vibrational spectroscopy on the samples synthesized by Pr Rafik Benrabaa and to take charge of writing this part.

Rose-Noëlle Vannier (Index h: 38, Index i10: 87), Professor and the Director of ENSCL-Lille. She obtained a doctorate from the University of Sciences and Techniques of Lille in 1992 and promoted to Professor of University in 2001, since 2002 she has been responsible for the "Oxidized Materials for Energy" research team at the UCCS. As a solid-state chemist, her research activities mainly focus on the research and characterization of oxide ion conductor for application in Solid Oxide Cells. In this paper, her contribution was mainly on the structural characterization of the catalysts at room temperature and variable temperatures.

Dr. Axel Löfberg obtained his Ph.D. in chemistry at the Free University of Brussels (ULB, Belgium) in 1996. He then joined the French CNRS as researcher at the Catalysis Laboratory, now UCCS, of the University of Lille. His research topics mostly concern the development of innovative contact modes and reactors for catalytic processes. This includes, oxide ion conducting membrane reactors, coated micro-structured catalytic reactors and non-steady state operating systems such as chemical looping. The reactions studied mostly concern the valorization of methane and alkanes (e.g., by dry reforming) and, more recently, selective oxidation of hydrogen sulfide or COV combustion.